



Integration of signals from different cortical areas in higher order thalamic neurons

Vandana Sampathkumar^{a,b} , Andrew Miller-Hansen^a , S. Murray Sherman^{a,1} , and Narayanan Kasthuri^{a,b,1}

^aDepartment of Neurobiology, University of Chicago, Chicago, IL 60637; and ^bBiosciences Division, Argonne National Laboratory, Lemont, IL 60439

Edited by Edward M. Callaway, Salk Institute for Biological Studies, La Jolla, CA, and approved June 15, 2021 (received for review March 2, 2021)

Higher order thalamic neurons receive driving inputs from cortical layer 5 and project back to the cortex, reflecting a transthalamic route for corticocortical communication. To determine whether or not individual neurons integrate signals from different cortical populations, we combined electron microscopy “connectomics” in mice with genetic labeling to disambiguate layer 5 synapses from somatosensory and motor cortices to the higher order thalamic posterior medial nucleus. A significant convergence of these inputs was found on 19 of 33 reconstructed thalamic cells, and as a population, the layer 5 synapses were larger and located more proximally on dendrites than were unlabeled synapses. Thus, many or most of these thalamic neurons do not simply relay afferent information but instead integrate signals as disparate in this case as those emanating from sensory and motor cortices. These findings add further depth and complexity to the role of the higher order thalamus in overall cortical functioning.

corticothalamic | sensorimotor | connectomics | electron microscopy

Until relatively recently, the view of thalamic neurons is that they simply relay information to the cortex with little or no integrative processing. This view drew heavily on lessons learned from the dominant model of the thalamus: the lateral geniculate nucleus (LGN), where receptive fields of geniculate relay cells closely match those of their retinal inputs. However, recent evidence has dramatically changed this view. There are three main reasons for this.

First, there is considerable evidence that modulatory input to the thalamus can strongly affect the response properties of thalamic relay cells (reviewed in ref. 1). Examples include the different tonic and burst firing modes, gain of response to driving inputs, etc.

Second, new evidence demonstrates that driver inputs that convey different types of peripheral sensory information converge onto single thalamic relay cells, therefore suggesting the possibility of significant integration of information prior to relaying to the cortex. These studies include evidence of retinal inputs with very different receptive fields converging onto single geniculate relay cells (2, 3), of driving inputs from retina and superior colliculus converging onto single geniculate relay cells (4), and of cortical layer 5 and brainstem driver inputs converging onto single cells of the posterior medial nucleus [POM (5)]. However, these examples are few, and each is limited in scale. There is also recent evidence that some thalamic relays may function without traditional driver input (6).

Third, the recent division of thalamic nuclei into two functional types, first order and higher order (reviewed in ref. 1), offers potentially new views on the extent to which thalamic neurons transform received information prior to transmission. Unlike first order thalamic relays, which receive driving input from a subcortical source (e.g., the retina for the LGN) and transmit that to the cortex, higher order relays receive inputs primarily from layer 5 of the cortex and thus serve as a transthalamic route for corticocortical communication. Therefore, the distinct functional organization of higher order thalamic relays offers an interesting substrate for thalamic integration of disparate information (7–9). Specifically, since higher order thalamic nuclei commonly receive overlapping projections from layer 5 neurons of multiple, distinct cortical areas (10), we can ask whether these multiple driving inputs containing different

types of information converge to synapse onto single relay cells. Because most of thalamus by volume seems to be higher order (1) and because most or all cortical areas send layer 5 projections to the thalamus as the afferent limb in transthalamic pathways (10), such convergence would have major significance for thalamocortical functioning.

To provide morphological evidence for such convergence, we employed modern viral tracing techniques to disambiguate multiple long-distance pathways in large volume serial electron microscope (EM) reconstructions (i.e., “connectomics”) in the mouse; by this approach, we could identify possible convergence of layer 5 inputs from somatosensory and motor cortices onto single relay cells of the POM, which is a higher order somatosensory thalamic nucleus. The viral tracing makes use of orthograde labeling of long pathways with an ascorbate peroxidase (APX) from the pea plant (11) that has allowed us to identify separately synaptic terminals from sensory and motor cortices onto neurons of the POM. Our results indicate significant convergence of presumptive driver inputs onto single thalamic neurons from layer 5 cells of disparate sensory and motor cortices.

Results

We injected two different types of adeno-associated virus (AAV) expressing the pea peroxidase APX (12–14) into the primary sensory (S1) and motor (M1) cortices of the same *Rbp4-cre* transgenic mouse (Fig. 1A). This mouse line expresses *cre* recombinase in layer 5 cortical neurons. One AAV construct targeted APX to the cytoplasm (APX-C) of layer 5 neurons and the other, to mitochondria (APX-M), thereby providing distinguishable labels for S1 and M1 layer 5 neurons and their synapses. Two mice were used. In one, APX-M was delivered to S1 and APX-C to M1; in the other, the labeling was reversed so that APX-C was delivered to S1 and APX-M to M1. In this way, we established a labeling protocol such that labeled synapses from two cortical regions could be

Significance

Higher order thalamic neurons receive input from layer 5 cells of different cortical regions. We address the issue of a possible convergence of information from these different cortical areas onto individual thalamic relay cells. We leverage advances in genetic labeling and serial electron microscopy to address this question. Using dual labeling to distinguish inputs from sensory and motor cortical areas, we provide evidence of integration of different cortical signals on single thalamic relay cells in the posterior medial nucleus. This provides insight into the complex functioning of thalamus.

Author contributions: V.S., A.M.-H., S.M.S., and N.K. designed research; V.S., A.M.-H., and N.K. performed research; V.S., S.M.S., and N.K. analyzed data; and V.S., A.M.-H., S.M.S., and N.K. wrote the paper.

The authors declare no competing interest.

This article is a PNAS Direct Submission.

Published under the [PNAS license](#).

¹To whom correspondence may be addressed. Email: msherman@bsd.uchicago.edu or bobby.kasthuri@gmail.com.

Published July 19, 2021.

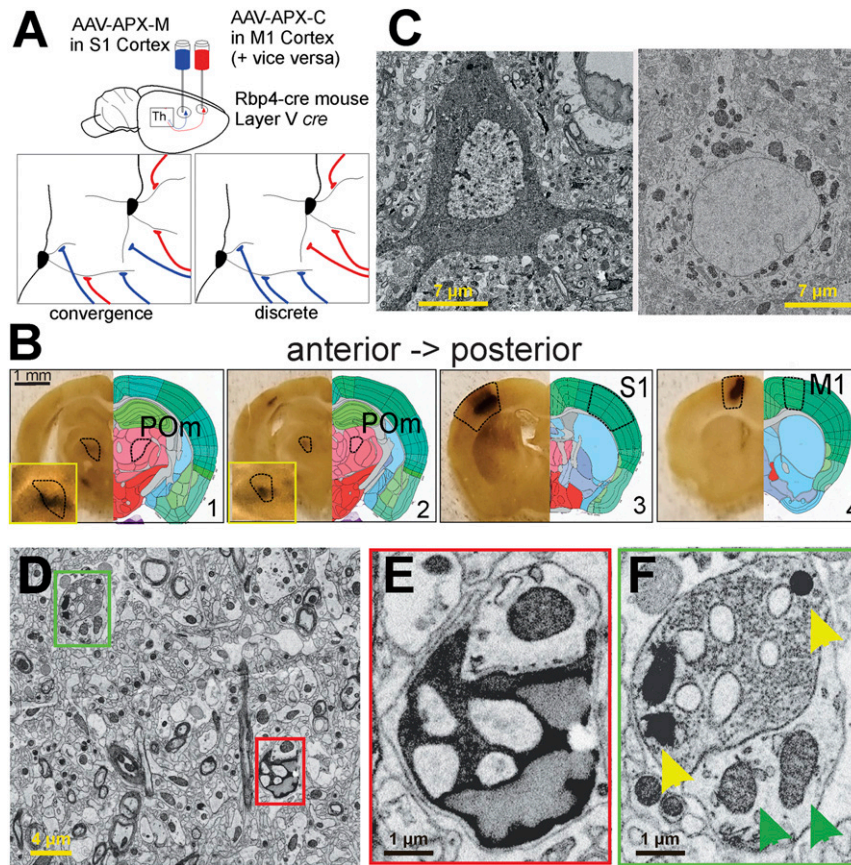


Fig. 1. Summary of experimental strategy. (A) We injected two types of AAV-expressing cre-dependent APX into the primary S1 or primary M1 cortices of two *Rbp4-cre* transgenic mice; this strategy limited expression of the label to layer 5 cells and in particular to layer 5 corticothalamic terminals in POM. In one mouse, as shown, the APX-C label was placed in M1 and the APX-M label in S1; in the other mouse (not shown) the APX-C label was placed in S1 and the APX-M label in M1. (B) DAB reactions in serial vibratome slices revealed APX expression in layer 5 cells of the cortical areas targeted as well as labeled layer 5 terminals in POM. (C) Electron micrographs of layer 5 neuronal cell bodies in S1 and M1 cortices show clearly distinguishable labeling when APX-C labels the cytoplasm (Left) and APX-M labels the mitochondria (Right). (D–F) Electron micrographs show two terminals near one another, one from layer 5 of M1 labeled with APX-C (red box in D and E) and the other from S1 labeled with APX-M (green box in D and F). (Insets) Higher resolution images of the synapses, and in F, yellow arrowheads point to synapses with APX-labeled mitochondria, and green arrowheads point to unlabeled mitochondria in other neurons.

unambiguously identified on POM neurons, and this allowed us to determine the presence and frequency of convergence of layer 5 input from two cortical areas onto individual POM neurons (Fig. 1A).

We found that this strategy worked: vibratome sections viewed with a light microscope showed dark staining at the injection sites in S1 and M1 as well as in the projection target, POM, indicating the APX-M and/or APX-C label (Fig. 1B). Serial EM of both cortical regions revealed neurons with either APX-C or APX-M labeling (Fig. 1C) as expected from the AAV construct injected in each area. The two distinct labels were also observed in synaptic terminals in POM, as expected, millimeters away from layer 5 cell bodies at either injection site (Fig. 1D). Indeed, boutons from S1 and M1 layer 5 neurons, only micrometers apart, could be easily disambiguated from each other and from unlabeled synapses in serial EM datasets of POM (Fig. 1E, APX-C; Fig. 1F, APX-M). Finally, an examination of the POM EM datasets revealed no sign of either POM neuronal soma or dendrites labeled with either APX-C or APX-M, suggesting that APX expression for both injections worked strictly in an orthograde fashion (Fig. 2). A lack of retrograde labeling with APX was also seen in our study of thalamocortical projections (11).

Fig. 2E–H shows the validity of the APX-M labeling method. To document the ability to identify confidently labeled mitochondria, we measured the optical density of each of the 66 mitochondria

(51 unlabeled and 15 labeled with APX-M) seen in five fields of view within the region of maximum APX labeling as described below. Fig. 2E shows one of these fields of view, and Fig. 2F–H shows the density distribution of this analysis: the transparency of APX-M-labeled mitochondria was far less than that of unlabeled mitochondria with no overlap at all of individual data points (Fig. 2H; $P = 5.6 \times 10^{-9}$ on a Mann–Whitney *U* test). Also, there was more variability in density readings among unlabeled than labeled mitochondria ($P = 7.2 \times 10^{-6}$ on an F-test). Finally, in our material regarding such APX-M labeling, we found consistency: in terminals and cell bodies, either all mitochondria were labeled or none was.

Qualitative Evidence of S1 and M1 Convergent Inputs to POM Neurons.

We found large synaptic terminals filled with synaptic vesicles that form axodendritic synapses in POM from both S1 and M1 (Fig. 3). Often, dendrites of POM neurons formed elaborate finger-like intrusions into these terminals, and multiple synapses from a single terminal were formed onto these intrusions (Fig. 3). In some cases, these synapses were also enclosed in a large glial sheath, and an unlabeled axon was also enclosed in the same glial sheath, indicative of a triadic synaptic arrangement (15). However, the vast majority of the large, labeled terminals were not involved in such elaborate synaptic configurations and formed simple axodendritic synapses.

Even casual inspection of EM stacks of POM revealed evidence of convergent S1 and M1 innervation onto individual dendrites of

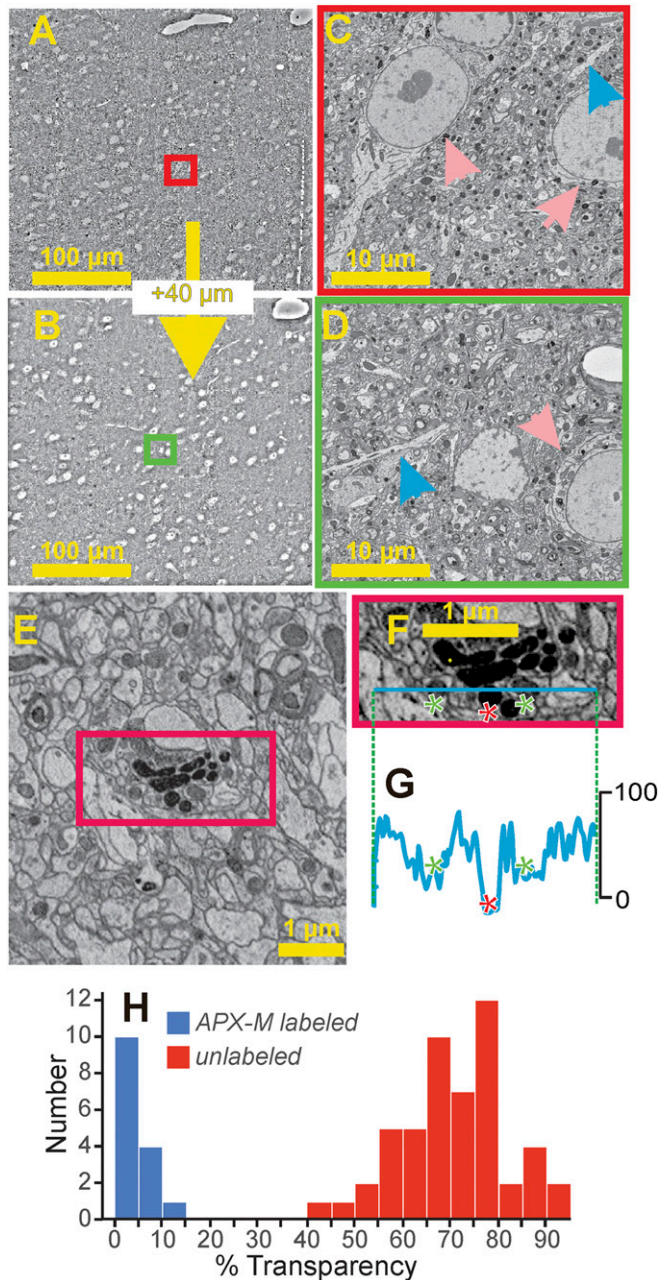


Fig. 2. Viral labeling with APX-C or APX-M. (A–D) APX does not retrogradely label neurons. Shown are two electron micrographs (A and B) 40- μm apart in a lower resolution electron microscopic stack (40 nm x, y, and z resolution) of POM from this dataset. There were no signs of APX-C or APX-M staining consistent with retrograde labeling in any cell body or dendrite in POM throughout the depth of the electron microscopic stack ($\sim 50\text{-}\mu\text{m}$ thick total). Higher resolution insets are shown from the two labeled fields of view (C and D; red and green rectangles), and blue and pink arrows point to representative unlabeled dendrites and soma, respectively. (E–H) Validation of APX-M labeling. (E) Field of view in which the transparency was measured for every mitochondrion. (F) Inset from red rectangle in E shows line along which transparencies were measured. The line crosses three mitochondria, two unlabeled (green asterisks) and one labeled with APX-M (red asterisk). (G) Transparency measures along the line indicated in F. (H) Frequency histogram of transparency readings for the mitochondria in five fields of view, one of which is shown in E.

POM neurons. Fig. 3 A–C shows an example of labeled S1 and M1 synapses within 2 μm of each other that innervate the same POM dendrite. Both S1 and M1 boutons were large as compared

to unlabeled synapses on the same dendrite. In a second animal, in which the labeling strategy was reversed, we easily found evidence of large S1 and M1 inputs synapsing within micrometers of each other on an unlabeled POM dendrite (Fig. 3 D and E), again showing that convergent innervation occurs. It thus seems clear in these two animals that, even without detailed EM reconstruction, synaptic input from layer 5 of S1 and M1 commonly converges onto POM neurons.

Quantitative Analysis of S1 and M1 Convergent Input to POM Neurons.

We performed quantitative analysis on the two animals based on detailed EM reconstructions of POM regions containing APX-C and APX-M labeling. We used slightly different approaches for each animal, including a different sampling strategy, and so these analyses are separately described here.

Case with APX-M Delivered to S1 and APX-C to M1. We annotated every potential S1 and M1 synapse in POM within a volume of $250 \times 250 \times 50 \mu\text{m}$ and found 315 S1 plus 111 M1 synapses therein; this region is shown in Fig. 4A. We selected a subvolume within this volume, designated by the green circle in Fig. 4A, having the highest density of both S1 and M1 synapses (213 S1 and 49 M1 synapses). Within this smaller volume, we reconstructed the dendritic arbors of every one of the 21 POM neurons with a cell body in that volume (Fig. 4B); this amounted to 2.74 mm of dendrite reconstructed. Finally, in order to estimate the density of labeled terminals, we selected a smaller volume (the yellow circle in Fig. 4A). Within this subvolume of highest labeling density, we estimate that the labeling frequency of S1 and M1 input relative to all synapses was low: labeled S1 and M1 synapses represented $\sim 0.5\%$ of all synapses (see *Materials and Methods*).

We found that synaptic convergence was common: of 21 reconstructed POM neurons, 11 were innervated by convergent S1 and M1 inputs. S1 innervation without clear M1 input was found on nine of

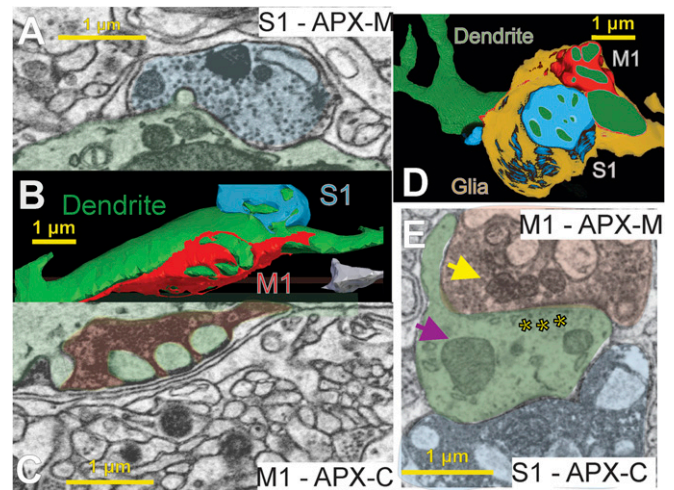


Fig. 3. Convergence of layer 5 M1 and S1 inputs onto individual POM dendrites. We found M1 and S1 synapses on the same POM dendrites in both animals. Shown are individual electron micrographs (A, C, and E) corresponding to three-dimensional reconstructions (B and D) of individual POM relay cell dendrites (green) from two mice. Both dendrites are postsynaptic to large layer 5 terminals from M1 (red) and S1 (blue) labeled with a different APX-targeted subcellular compartment in each animal. In A through C, the animal was injected with APX-C in M1 and APX-M in S1, and for D and E, the labels were switched, APX-C in S1 and APX-M in M1. Each input and the dendrite are shaded in the electron micrographs (A, C, and E) corresponding to their colors in the reconstructions (B and D). Synaptic vesicles can be clearly seen (A, C, and E), and a clear postsynaptic density is shown in E (asterisks). Finally, examples of mitochondria labeled with APX (yellow arrow) as compared to unlabeled mitochondria in the postsynaptic dendrite (purple arrow) are shown in E.

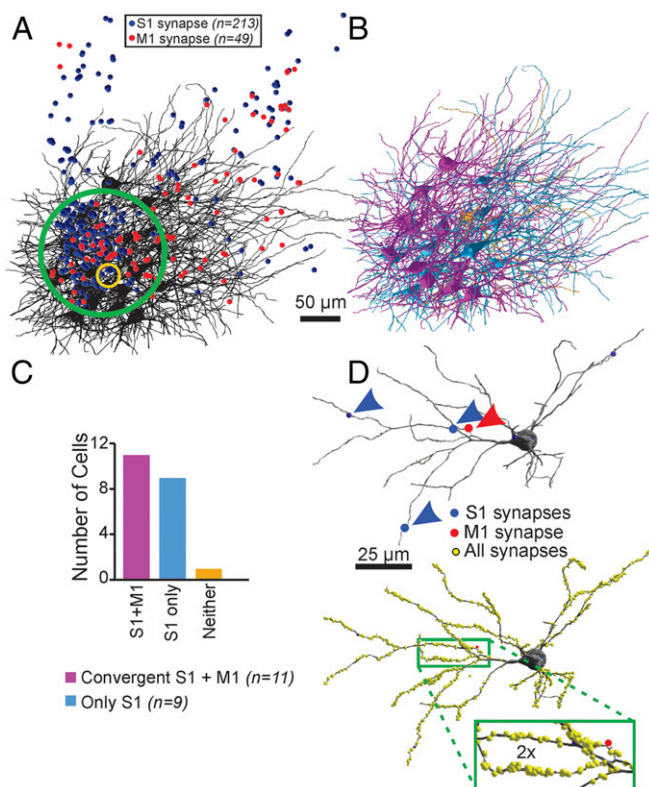


Fig. 4. Convergence of M1 and S1 inputs on single thalamic neurons in POM is common. (A) In the mouse with APX-C labeling from M1 and APX-M labeling from S1, we first identified regions (green circle) in the electron microscopic datasets with the highest concentrations of labeled S1 (blue circles) and M1 (red circles) terminals. The yellow circle indicates the region in which detailed measure of all synapses identified to determine synaptic density. (B) In that volume, we reconstructed 2.74 mm of the full dendritic arbor of all 21 neurons and identified all S1- and M1-labeled inputs on each neuron. (C) We found that 20 of the 21 neurons had at least a single input from S1 (cyan neurons) and that 10 of these showed a second input from the M1 cortex (purple). We found no examples of innervation of these POM neurons by M1 and not S1 and only one example of a neuron that received neither labeled input (orange neuron in B and C). (D) For subset of four neurons with convergent input, we determined the location and size of all synapses labeled or unlabeled (yellow spheres). An example is shown, and unlabeled synapses are indicated as yellow circles.

the 21 POM neurons, and one of the neurons had no labeled S1 or M1 input. We found no examples of POM neurons innervated by M1 alone (Fig. 4B); that is, every synapse from M1 was made on a neuron that also received synaptic input from S1. It is also noteworthy that in the 20 neurons with labeled S1 and/or M1 inputs, there were also numerous synaptic inputs from unlabeled large terminals (see below).

We then asked whether and how S1- and M1-labeled synapses differed from unlabeled synapses or from each other on POM dendrites. To do this, we reconstructed 1,820 unlabeled synapses throughout the dendritic arbor of 4 POM neurons with convergent S1 and M1 inputs (an example neuron is shown in Fig. 4C and D). The cell bodies of these POM neurons were nearly free of synaptic input, typically having only two to three each, a finding in agreement with observations of inputs to relay cells of the cat's LGN (16, 17).

We plotted for every synapse, labeled and unlabeled, the diameter of the axonal bouton, the distance of the synapse from the cell body along the dendritic arbor, and the dendritic branch number (Fig. 5A and B). We found that labeled synapses from both S1 and M1 ($n = 104$) differed statistically from unlabeled synapses on all three measurements. Compared to unlabeled terminals: the labeled

terminals were more than twice as large in diameter ($3.2 \pm 1.1 \mu\text{m}$ versus $1.4 \pm 0.16 \mu\text{m}$; $P = 5.4 \times 10^{-45}$ on a Mann-Whitney U test; Fig. 5B); they occur closer to the cell body ($65.1 \pm 3.1 \mu\text{m}$ versus $83.1 \pm 0.9 \mu\text{m}$; $P = 1.1 \times 10^{-7}$ on a Mann-Whitney U test; Fig. 5B), and they are more often on proximal dendritic branches based on the mean dendritic branch number (3.5 versus 5.2 ; $P = 2.8 \times 10^{-7}$ on a Mann-Whitney U test; Fig. 5A). While there was a clear difference in the mean size and location of labeled M1 and S1 synapses relative to unlabeled, there was also considerable overlap (see Discussion). We found no obvious relationship between the number of labeled M1 inputs relative to that of labeled S1 inputs on convergent POM neurons (Fig. 5C) nor did we find any between the length of dendrite reconstructed and the extent of convergence (Fig. 5D; $P = 0.352$, $n = 33$ neurons on a Mann-Whitney U test).

We looked for differences between POM neurons showing convergent S1 and M1 input and those that did not. There was no difference in either cell body diameter (for convergent neurons, $14.7 \pm 1.3 \mu\text{m}$; for nonconvergent neurons, $15.1 \pm 2.0 \mu\text{m}$; $P = 0.33$ on a Mann-Whitney U test). Likewise, a Sholl analysis of dendritic structure revealed no difference ($P = 0.17$ on a Kolmogorov-Smirnov test, see Materials and Methods).

Finally, we examined the 11 POM neurons showing convergence for obvious patterns in the location of S1 and M1 inputs relative to each other and/or those of other comparably large unlabeled terminals (i.e., those $\geq 2 \mu\text{m}$ in diameter, Fig. 6). We first estimated the frequency of APX labeling of such large unlabeled as well as APX-labeled terminals in our EM datasets. On four neurons for which we identified every synapse, we found that $3.3 \pm 1.7\%$ of all synapses were made by these terminals (10/974, 21/615; 30/696, 11/431). For the 21 neurons we examined for convergence from S1 and M1, we determined that the contribution of APX-labeled (both APX-C and APX-M) terminals to all such large unlabeled terminals was 10.8 ± 5.4 terminals ($17.4 \pm 26.4\%$), and therefore we estimated that $\sim 0.5\%$ of all large terminal synapses on POM neurons were APX labeled in our EM datasets.

We found little evidence of obvious patterns in the dendritic distribution of these terminals. Sometimes, convergence occurred on POM neurons with numerous large unlabeled terminals (Fig. 6C, I, and J) and sometimes on POM neurons with few such large terminals (Fig. 6B, D, and K). Sometimes, convergent APX-labeled synapses from the two areas were extremely close to each other on dendrites (Fig. 6B, F, and K), but in other examples, S1 and M1 inputs were on completely different parts of the dendritic arbor (Fig. 6C, H, and I). Labeled S1 inputs were in some cases the dominant population among large input terminals on POM neurons showing convergence (Fig. 6D and E), and in others, S1 and M1 inputs were a very small fraction of the large inputs (Fig. 6C, I, and J). **Case with APX-C Delivered to S1 and APX-M to M1.** We also obtained data from a second animal with reversed labeling from the above case so that APX-C was delivered to layer 5 neurons of S1 and APX-M to those of M1. Our goal here was to confirm the main observation of convergent S1 and M1 input to individual POM neurons, and so the level of quantitative analysis was largely limited to that topic. We identified POM neurons with labeled M1 synaptic input for further analysis because in the example above, POM neurons with convergent input had fewer M1 inputs. In this way, we reconstructed the dendritic arbors of 12 POM neurons postsynaptic to a labeled M1 input and again found that 66% (8/12) also had a labeled S1 input, establishing convergent input for these eight neurons. Finally, we found convergence on POM neurons to be independent of the amount of dendrite traced (Fig. 5D) ($P = 0.21$ on a Mann-Whitney U test, $n = 33$ neurons).

Discussion

We leveraged advances in automated serial EM paired with electron dense genetic labeling using APX to analyze long-distance connections from two cortical regions, S1 and M1, to the POM

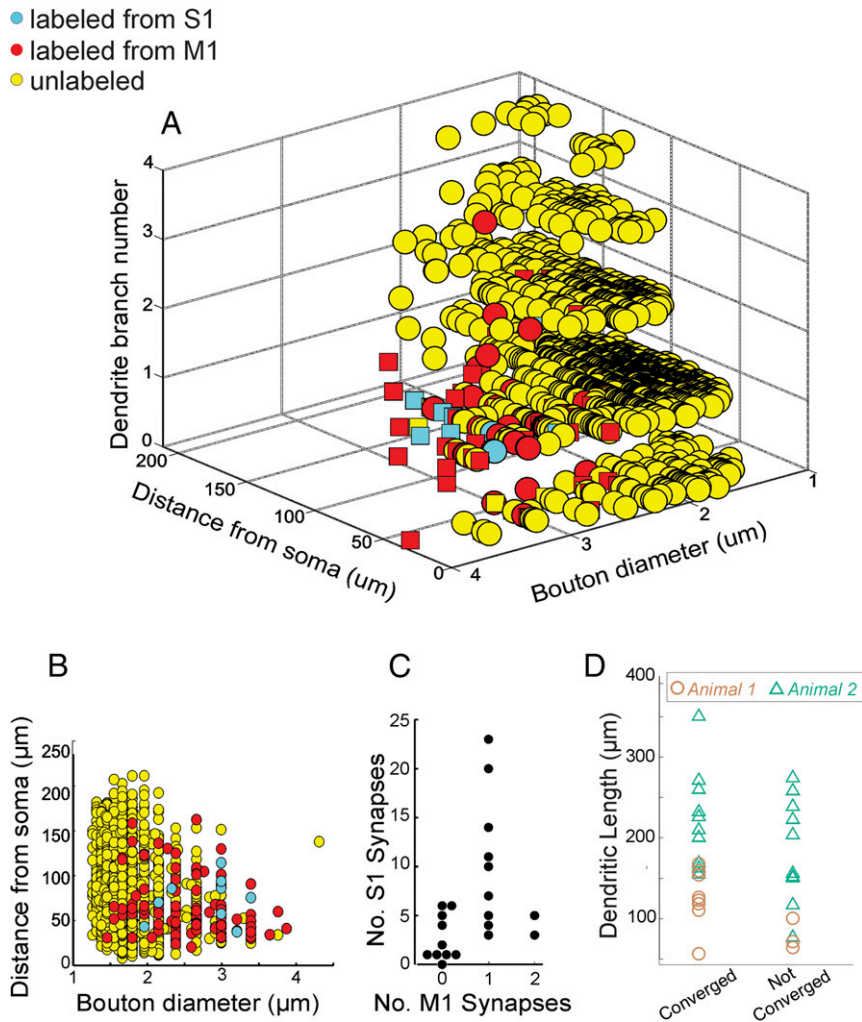


Fig. 5. Quantitative analyses of labeled versus unlabeled inputs. We reconstructed the locations and terminal size of all labeled synapses (blue: APX-M from S1; red: APX-C from M1) and unlabeled synapses (yellow) on four of the POm neurons, with one example indicated in Fig. 4D. On the remaining 18 neurons from Fig. 4, we reconstructed labeled and large (>2 μm in diameter) unlabeled terminals throughout the dendritic tree. (A) Three-dimensional plot showing for each synapse the size of the axonal terminal, the distance from the soma, and the number of dendritic branch points from the soma. Squares correspond to values from the neuron in Fig. 4D. (B) Compared to unlabeled synapses, labeled synapses from both M1 and S1 had larger terminals and were more proximally located (see text for details). (C) We found little correlation between the number of S1 inputs received by a neuron relative to the number of M1 inputs (C) and on the amount of dendrite traced relative to whether neurons showed convergence or not (D).

of the thalamus. APX was expressed specifically in layer 5 neurons of the cortex through the use of *cre* recombinase-dependent AAVs in *Rbp4-cre* mice, a line that expresses *cre* in layer 5 neurons. We found that the labeling strategy works extremely well: labeled synapses from the different cortices were clearly identified in the same large volume EM dataset of POm, millimeters away from their cell bodies of origin and without signs of reduction in labeling from diffusion or pathological changes to the tissue at the ultrastructural level. We also found that the labeling was orthograde only, avoiding problems associated with retrograde labeling. Genetic labeling offers the advantage that multiple types of neurons, in this case layer 5 neurons from disparate cortical regions, can be labeled and their axons and synapses easily distinguished from each other and those from unlabeled neurons.

We found that convergence of synaptic inputs from M1 and S1 layer 5 neurons onto individual POm neurons to be quite common. Putting together the results from both cases, we reconstructed 33 POm neurons in the area of S1 and M1 terminal overlap and found that 19 of these neurons received convergent S1 and M1 input. We found certain innervation patterns in our results. Labeled terminals

on POm cells were larger and were located more proximally both in terms of distance from the soma as well as branch number than were unlabeled terminals (Fig. 5). However, despite the statistical differences noted, Fig. 5 also shows considerable overlap between labeled and unlabeled terminals both in terms of size, with a tail of larger labeled terminals, as well as dendritic contact location. This is consistent with prior studies of terminals identified as driver: an overlap in sizes between driver and modulator terminals, with the driver population having an extended distribution of larger terminals, has been shown (18–20), and scattered retinal (driver) terminals have been found more peripherally on relay cell dendrites (17, 21). We saw no obvious spatial relationship between the relative locations of S1 and M1 terminals on individual POm dendritic arbors.

Some Technical Limitations. We recognize certain limitations to the interpretation of our data analysis. We cannot assume that all cortical layer 5 cells contributing to the pathways under study were successfully labeled, and, of course, other cortical regions innervating the POm (e.g., secondary somatosensory cortex and the spinal nucleus of the fifth nerve) could have contributed to the population of

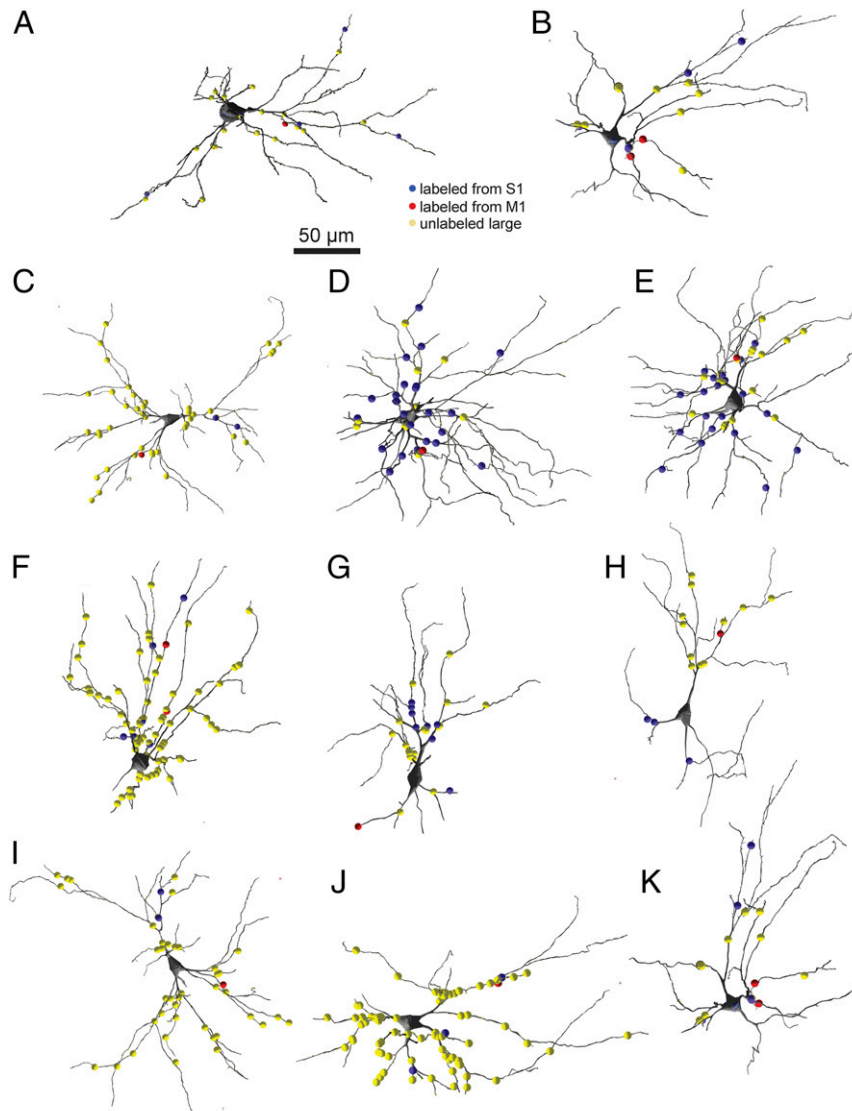


Fig. 6. Distribution of S1, M1, and large unlabeled synapses on POM dendrites. (A–K) Shown are the locations of large (>2 μm in diameter) unlabeled synapses (yellow circles), S1 synapses (blue circles), and M1 synapses (red circles) within the full reconstructed dendritic arbors of the 11 neurons with convergent input from one mouse. See text for details.

unlabeled cortical terminals in our study. Related to this, we cannot exclude the possibility that we have selectively labeled a particular subpopulation of layer 5 corticothalamic neurons, and unlabeled layer 5 neurons from either cortical region might exhibit properties different from those reported here. Finally, we likely reconstructed only a fraction, albeit in some cases a large fraction, of the dendritic arbor of individual POM neurons. It is therefore likely that our analysis undersampled the totality of cortical input. However, these limitations only underscore the conclusion that convergence by different cortical regions on individual thalamic neurons is common; that is, with complete labeling of all M1 and S1 cortical inputs and full reconstructions of dendritic arbors, the numbers of POM neurons receiving convergent input would likely be larger than reported here.

Convergence of Driver Inputs. Glutamatergic inputs in the cortex and thalamus have been classified into drivers and modulators based on a number of physiological and morphological criteria, the idea being that the former are the main conduits of information transfer, whereas the latter provide modulatory functions that are more

topographically organized and represent thalamocortical influence, since they frequently arise from the thalamus or cortex, when compared to classical modulatory pathways that are generally diffusely organized and derive from brainstem (reviewed in refs. 1, 7, and 22). For several reasons, we suggest that the layer 5 corticothalamic synapses described here represent driver input to POM cells. First, evidence from multiple sources indicate generally that, whereas layer 6 cortical input to the thalamus acts as a modulator, layer 5 corticothalamic input is a driver (1, 7, 22). Specific evidence for a layer 5 driver input from S1 to POM exists (18, 23), although such evidence for the M1 to POM pathway is currently lacking. However, we emphasize that, whereas identifying layer 5 corticothalamic inputs as driver may be relatively straightforward, the interpretation of these as the source of information brought to the thalamus for a relay to the cortex remains a hypothesis, and recent evidence suggests that some thalamic relays may not involve such driver input (6). We nonetheless feel that using this driver/modulator framework to interpret our data are useful as long as it is recognized as somewhat speculative.

An elaboration of receptive field properties as occurs in the visual system via retinal and cortical circuitry is thought to result from a convergence of driver inputs representing somewhat different properties: thus, simple cell receptive fields are formed by a convergence of geniculate inputs, each representing slightly different receptive field locations, and that of complex cells by a convergence of inputs from simple cells (24, 25). It used to be thought that such convergence of disparate driver input was not a feature of thalamic circuitry. For instance, in the cat, the receptive field of a geniculate neuron closely resembles that of its retinal input, which is the driver input for these cells, because there is little or no convergence in retinogeniculate circuitry. In this regard, the thalamus was seen as mainly a gated relay, with little or no elaboration of information.

However, recent data from the mouse indicates a need to reconsider this notion. Not only is there now evidence for significant convergence of retinogeniculate input (3) (but see ref. 2), but there are also limited and isolated examples of convergence from different sources of synapses from large terminals thought to be drivers onto single thalamic neurons: in one case from the retina and superior colliculus (4) and in the other, from the brainstem and cortex (5).

Our data extend these scattered and limited observations in several ways. First, ours is a demonstration of significant convergence of presumed driver input to thalamic neurons from different cortical areas, and the fact that the source of convergence is cortical suggests a role of thalamic information processing underlying more cognitive functioning than previously suggested. Second, our quantitative analysis of multiple cells and synapses indicates that this convergence is fairly ubiquitous and not perhaps a rare accident of circuit formation.

Finally, our finding from the first animal is that roughly half of the POM cells in the region of overlap of APX-C- and APX-M-labeled terminals receive input from M1, and the rest do not. These corticothalamic projections are likely organized in a topographic manner, and the fact that the analyzed zone of POM contained a continuous pattern of input from M1 suggests that the failure of finding inputs from M1 to many POM cells is not due to topographic misalignment. This is rather like the case in the A layers of the cat LGN in which X and Y cells are arranged cheek by jowl, and yet, with rare exceptions, each receives only one type of retinal (X or Y) input (26, 27). Indeed, the pattern we have seen, like that for the cat LGN, suggests a surprising level of specificity beyond topography, at least for the M1 projection to POM.

Paucity of Driver Inputs to Thalamus. As noted above, driver inputs are associated with large terminals. As such, we have reported that only about 3% of synaptic input to POM cells are carried by such large terminals. Whereas this may seem like a very small number, it is in accord with other estimates for driver inputs to the thalamus. For instance, in the first order visual and somatosensory thalamic nuclei (LGN and ventral posterior nucleus, or VPN) of mice, rats, and cats, estimates of the percentage of large and presumed driver synapses vary from about 5 to 15% (16, 28–30), and it has been suggested that the higher estimates are due to not taking into account sampling biases in favor of counting larger terminals (16). Interestingly, when comparisons in the cat were made between first and higher order thalamic nuclei (i.e., LGN versus pulvinar, VPN versus POM, and the ventral versus dorsal divisions of the medial geniculate nucleus), higher order nuclei had a consistently lower percentage of presumed driver synapses (31, 32), with the number being as low as 2% for the pulvinar (31). This first order/higher order difference has also been documented for several thalamic pairs in the rat (33). Thus, our data from the mouse for the higher order POM are in rough agreement with these data from other studies.

Conclusions

As noted previously, higher order thalamic relays have only relatively recently been identified as a key link in corticocortical communication via transthalamic cortico-thalamo-cortical circuitry that is organized in parallel to direct corticocortical connections (reviewed in refs. 1 and 7). We are just beginning to scratch the surface of understanding the functional significance of these transthalamic pathways and the role of higher order thalamic nuclei. The evidence presented here indicates that the nature of messages transmitted by these nuclei is not a simple relay of information from one cortical area to another but rather involves significant integration of information from multiple cortical areas. Indeed, our observation that, in addition to identified inputs from S1 and M1, POM neurons also receive inputs from many large, presumed driver inputs from unknown sources suggests an even greater integration of information than our data directly show. This functional feature of higher order thalamus needs to be considered in the role of these transthalamic pathways for cortical functioning writ large.

Materials and Methods

All procedures were performed in accordance with the University of Chicago Institutional Animal Use and Care Committee. Data were obtained from two male Rbp4-cre transgenic mice.

Viral Injections. We injected two types of AAV using stereotactic coordinates to target the primary somatosensory cortex (from bregma dorsal–ventral: –0.5 mm, medial–lateral: 3.0 mm, anterior–posterior: –0.8 mm) and motor cortex (dorsal–ventral: –0.5 mm, medial–lateral: 1.1 mm, anterior–posterior: +1.1) of transgenic mice aged 3 to 4 wk (18). A volume of 200 to 300 nl each virus was injected to express the pea peroxidase APX 2.0 (12) in a cre-dependent fashion with one version targeting APX to the cytoplasm (APX-C) and the other to mitochondria (APX-M). APX-M was constructed by subcloning APX2-Mito sequence from mito-V5-APX2 plasmid (mito_V5-APX2 was a gift from Alice Ting, Stanford University, Stanford, CA, Addgene plasmid no. 72480; <http://n2t.net/addgene:72480>; RRID: [Addgene_72480](https://identifiers.org/RRID:Addgene_72480)) into AscI and NheI restriction sites of AAV-CAG-DIO-APX2NES plasmid (AAV-CAG-DIO-APX2NES was a gift from Joshua Sanes, Harvard University, Cambridge, MA, Addgene plasmid no. 79907; <http://n2t.net/addgene:79907>; RRID: [Addgene_79907](https://identifiers.org/RRID:Addgene_79907)). The plasmid was packaged into rAAV9 at the Gene Therapy Center virus Vector Core facility at the University of North Carolina Chapel Hill. One transgenic mouse was injected with AAV-APX-C and AAV-APX-M in M1 and S1, respectively, and we reversed the injections in a second Rbp4-cre mouse to place AAV-APX-C and AAV-APX-M in S1 and M1, respectively. All mice were returned to their cages for 4 wk to allow for transgene expression and transport of the label and then processed for peroxidase staining and large volume EM reconstruction as described below. We waited 4 wk for expression of APX labeling based on prior work (34) as well as our own experience (11).

We directed the S1 and M1 injections to both include regions mapped to the mystacial whiskers as previously defined (35). This provided sufficient topographical alignment to result in the overlap of S1 and M1 terminals in POM that we observed.

Electron Microscopy. Mice were deeply anesthetized with pentobarbital (60 mg/kg intraperitoneal; to be nonresponsive to toe pinch) and transcardially perfused with 10 mL 0.1 M cacodylate buffer followed by 20 mL 2% paraformaldehyde and 2.5% glutaraldehyde in 0.1 M cacodylate buffer. Each brain was removed, and coronal sections (350 μ m thick) were cut using a vibratome. The sections were then stained with Di-Amino-Benzidine (DAB) and H₂O₂ to visualize APX labeling (14). The samples were evaluated at the macro scale for the intensity of the DAB reaction and its localization to the appropriate brain regions, namely M1 and S1 cortices and the POM. POM was distinguishable by eye, and S1 and M1 were localized as indicated in Fig. 1B. Samples with appropriate staining were subsequently stained with multiple rounds of osmium and reduced osmium en bloc uranium and lead, dehydrated, and then plastic embedded (36). Approximately 3,000 40- to 45-nm thick ultra-thin serial sections were cut with a cross-section of 1.7 \times 1.1 mm, collected on Kapton tape, attached to wafers, and carbon coated (13).

Ultra-thin sections were then imaged with a backscatter detector on a Zeiss Gemini SEM 300 and ATLAS software or with a T1 segmented lower lens detector on Volumescope (Thermo Fisher Scientific) and Maps version 3.10. Low-resolution data were imaged at 20 nm x and y pixel resolution, and large fields of view were collected by montaging individual tiles.

This involved 2 × 2 tiles each of 12 or 10k pixels stitched together with a 10% overlap to produce a 22.8k × 22.8k or 19k × 19k pixel image. Because of the 10% overlap, the result was 22.8k × 22.8k or 19k × 19k pixels rather than the 24k × 24k or 20k × 20k. Fine-resolution EM imaging was done at 6 nm resolution and was a single tile field of view (10k × 10k pixels). Imaging rates were 0.8 to 1 μs per pixel for low-resolution images and 1.6 μs per pixel for fine-resolution images. Individual tiles for lower resolution datasets were stitched two-dimensionally and linearly aligned three-dimensionally using a plugin, TrakEM2 (37), in the open-source image processing program *ImageJ*. Fine-resolution image stacks often required further alignment using non-linear deformations of the image, which was performed using the program *aligntk* (<https://mmbios.pitt.edu/about-us/acknowledgements>) on Cooley at Argonne National Laboratory.

Identifying APX-M Labeling. To verify the validity of APX-M labeling, we measured the optical density of every mitochondrion in five fields of view like that shown in Fig. 2H. First, for each field of view, we determined gray scale values of cytoplasm alone, with no subcellular organelles, as a baseline for accommodating potential differences in the image acquisition that can subtly affect brightness and contrast. These mean gray scale values for cytoplasm differed by less than 2% across the five fields of view, allowing us to simply pool imaging data across these fields of view. We then measured optical density for all mitochondria in these fields using the line scan feature on *ImageJ* to produce the data shown in Fig. 2.

Tracing Neurons and Their Connections. For identifying APX-C and APX-M synapses, reconstructing the dendritic arbors of postsynaptic targets, and identifying and characterizing their synaptic features (e.g., measuring axonal terminal diameters), we used Knossos annotation software (38). For

determining the density of APX-C- and APX-M-labeled terminals and synapses in POM, in a smaller volume of 3,991 μm³ within the dense S1 and M1 labeling region, we found 1,601 unlabeled synapses and seven labeled, four from S1 and three from M1 synapses, giving a labeling frequency of 7/1,608.

Determining labeled versus unlabeled mitochondria was done primarily by visual inspection since APX-labeled mitochondria are far darker than unlabeled (Fig. 2). At synapses where the terminal did not contain a mitochondrion, we traced the parent axon back until at least two mitochondria were found; if both were labeled, we considered the terminal labeled from the cortex, and vice-versa. As noted in *Results*, we found that in our material, if a given process or cell body had labeled mitochondria, all were labeled, and if unlabeled, none was labeled.

We performed Sholl ring analyses using an *ImageJ* plugin and the neuronal skeletons from our Knossos tracings (39–41). Briefly, we calculated the number of dendritic branch points as a function of distance from the soma for each thalamic neuron traced.

Statistical analyses (Mann–Whitney *U*, χ^2 , Kolmogorov–Smirnov, or ANOVA tests) were performed on the data using custom software in MATLAB.

Data Availability. All study data are included in the main text.

ACKNOWLEDGMENTS. N.K. and V.S. are supported from a technical award from the McKnight foundation, a Brain Initiative of the NIH (U01 MH109100), and an NSF Neuro Nex grant. A.M.-H. and S.M.S. are supported by a NIH grant from the National Institute of Neurological Disorders and Stroke (NINDS) (NS094184) and National Eye Institute (NEI) (EY022388). N.K. and S.M.S. are supported by an NIH grant from the NINDS (NS113922). Finally, A.M.-H. is supported an NIH grant from the NEI (EY028812).

1. S. M. Sherman, R. W. Guillery, *Functional Connections of Cortical Areas: A New View from the Thalamus* (MIT Press, Cambridge, MA, 2013).
2. E. Y. Litvina, C. Chen, Functional convergence at the retinogeniculate synapse. *Neuron* **96**, 330–338.e5 (2017).
3. J. L. Morgan, D. R. Berger, A. W. Wetzel, J. W. Lichtman, The fuzzy logic of network connectivity in mouse visual thalamus. *Cell* **165**, 192–206 (2016).
4. M. E. Bickford, N. Zhou, T. E. Krahe, G. Govindaiah, W. Guido, Retinal and tectal “driver-like” inputs converge in the shell of the mouse dorsal lateral geniculate nucleus. *J. Neurosci.* **35**, 10523–10534 (2015).
5. A. Groh *et al.*, Convergence of cortical and sensory driver inputs on single thalamocortical cells. *Cereb. Cortex* **24**, 3167–3179 (2014).
6. M. E. Bickford, Thalamic circuit diversity: Modulation of the driver/modulator framework. *Front. Neural Circuits* **9**, 86 (2016).
7. S. M. Sherman, Thalamus plays a central role in ongoing cortical functioning. *Nat. Neurosci.* **19**, 533–541 (2016).
8. M. J. Arcaro, M. A. Pinsk, J. Chen, S. Kastner, Organizing principles of pulvino-cortical functional coupling in humans. *Nat. Commun.* **9**, 5382 (2018).
9. M. M. Halassa, S. Kastner, Thalamic functions in distributed cognitive control. *Nat. Neurosci.* **20**, 1669–1679 (2017).
10. J. A. Prasad, B. J. Carroll, S. M. Sherman, Layer 5 corticofugal projections from diverse cortical areas: Variations on a pattern of thalamic and extra-thalamic targets. *J. Neurosci.* **40**, 5785–5796 (2020).
11. V. Sampathkumar, A. Miller-Hansen, S. Murray Sherman, N. Kasthuri, An ultrastructural connectomic analysis of a higher-order thalamocortical circuit in the mouse. *Eur. J. Neurosci.* **53**, 750–762 (2021).
12. J. D. Martell, T. J. Deerinck, S. S. Lam, M. H. Ellisman, A. Y. Ting, Electron microscopy using the genetically encoded APEX2 tag in cultured mammalian cells. *Nat. Protoc.* **12**, 1792–1816 (2017).
13. N. Kasthuri *et al.*, Saturated reconstruction of a volume of neocortex. *Cell* **162**, 648–661 (2015).
14. S. S. Lam *et al.*, Directed evolution of APEX2 for electron microscopy and proximity labeling. *Nat. Methods* **12**, 51–54 (2015).
15. S. M. Sherman, Interneurons and triadic circuitry of the thalamus. *Trends Neurosci.* **27**, 670–675 (2004).
16. S. C. Van Horn, A. Erişir, S. M. Sherman, Relative distribution of synapses in the A-laminae of the lateral geniculate nucleus of the cat. *J. Comp. Neurol.* **416**, 509–520 (2000).
17. J. R. Wilson, M. J. Friedlander, S. M. Sherman, Fine structural morphology of identified X- and Y-cells in the cat’s lateral geniculate nucleus. *Proc. R. Soc. Lond. B Biol. Sci.* **221**, 411–436 (1984).
18. C. Mo, S. M. Sherman, A sensorimotor pathway via higher-order thalamus. *J. Neurosci.* **39**, 692–704 (2019).
19. C. Mo, I. Petrof, A. N. Viaeña, S. M. Sherman, Synaptic properties of the lemniscal and paralemniscal pathways to the mouse somatosensory thalamus. *Proc. Natl. Acad. Sci. U.S.A.* **114**, E6212–E6221 (2017).
20. A. N. Viaeña, I. Petrof, S. M. Sherman, Properties of the thalamic projection from the posterior medial nucleus to primary and secondary somatosensory cortices in the mouse. *Proc. Natl. Acad. Sci. U.S.A.* **108**, 18156–18161 (2011).
21. J. E. Hamos, S. C. Van Horn, D. Raczowski, S. M. Sherman, Synaptic circuits involving an individual retinogeniculate axon in the cat. *J. Comp. Neurol.* **259**, 165–192 (1987).
22. S. M. Sherman, R. W. Guillery, On the actions that one nerve cell can have on another: Distinguishing “drivers” from “modulators”. *Proc. Natl. Acad. Sci. U.S.A.* **95**, 7121–7126 (1998).
23. I. Reichova, S. M. Sherman, Somatosensory corticothalamic projections: Distinguishing drivers from modulators. *J. Neurophysiol.* **92**, 2185–2197 (2004).
24. D. H. Hubel, T. N. Wiesel, Receptive fields, binocular interaction and functional architecture in the cat’s visual cortex. *J. Physiol.* **160**, 106–154 (1962).
25. D. H. Hubel, T. N. Wiesel, Receptive fields of single neurones in the cat’s striate cortex. *J. Physiol.* **148**, 574–591 (1959).
26. S. M. Sherman, P. D. Spear, Organization of visual pathways in normal and visually deprived cats. *Physiol. Rev.* **62**, 738–855 (1982).
27. W. M. Usrey, H. J. Alitto, Visual functions of the thalamus. *Annu. Rev. Vis. Sci.* **1**, 351–371 (2015).
28. S. Cavdar *et al.*, Comparison of numbers of interneurons in three thalamic nuclei of normal and epileptic rats. *Neurosci. Bull.* **30**, 451–460 (2014).
29. M. E. Bickford *et al.*, Synaptic development of the mouse dorsal lateral geniculate nucleus. *J. Comp. Neurol.* **518**, 622–635 (2010).
30. X.-B. Liu, C. N. Honda, E. G. Jones, Distribution of four types of synapse on physiologically identified relay neurons in the ventral posterior thalamic nucleus of the cat. *J. Comp. Neurol.* **352**, 69–91 (1995).
31. S. Wang, M. A. Eisenback, M. E. Bickford, Relative distribution of synapses in the pulvina nucleus of the cat: Implications regarding the “driver/modulator” theory of thalamic function. *J. Comp. Neurol.* **454**, 482–494 (2002).
32. S. C. Van Horn, S. M. Sherman, Fewer driver synapses in higher order than in first order thalamic relays. *Neuroscience* **146**, 463–470 (2007).
33. S. Çavdar, H. Hacıoğlu, S. Şırvancı, E. Keskinöz, F. Onat, Synaptic organization of the rat thalamus: A quantitative study. *Neurosci. Sci.* **32**, 1047–1056 (2011).
34. M. Joesch *et al.*, Reconstruction of genetically identified neurons imaged by serial-section electron microscopy. *eLife* **5**, 5 (2016).
35. V. Sreenivasan *et al.*, Movement initiation signals in mouse whisker motor cortex. *Neuron* **92**, 1368–1382 (2016).
36. Y. Hua, P. Laserstein, M. Helmstaedter, Large-volume en-bloc staining for electron microscopy-based connectomics. *Nat. Commun.* **6**, 7923 (2015).
37. A. Cardona *et al.*, TrakEM2 software for neural circuit reconstruction. *PLoS One* **7**, e38011 (2012).
38. K. M. Boergens *et al.*, webKnossos: Efficient online 3D data annotation for connectomics. *Nat. Methods* **14**, 691–694 (2017).
39. T. A. Ferreira *et al.*, Neuronal morphometry directly from bitmap images. *Nat. Methods* **11**, 982–984 (2014).
40. M. Helmstaedter, K. L. Briggman, W. Denk, High-accuracy neurite reconstruction for high-throughput neuroanatomy. *Nat. Neurosci.* **14**, 1081–1088 (2011).
41. J. Schindelin *et al.*, Fiji: An open-source platform for biological-image analysis. *Nat. Methods* **9**, 676–682 (2012).